Evanescent wave cavity ring-down spectroscopy for probing surface processes

Andrew C.R Pipino [1], Jeffrey W. Hudgens, Robert E. Huie

Physical and Chemical Properties Division, Chemical Science and Technology Laboratory, National Institute of Standards and Technology, Gaithersburg, MD 20899, USA

Abstract

Sub-monolayer detection of adsorbed I_2 is demonstrated with the cavity ring-down technique by using intra-cavity total-internal reflection to generate an evanescent field that probes the adsorption process. A precision, fused-silica Pellin-Broca prism with ultra-smooth facets (surface roughness ~ 0.05 nm r.m.s) is employed to provide the intra-cavity TIR. The known cross-section for the $^1\Sigma_g^+ \rightarrow ^3\Pi_u$ transition of I_2, which is largely invariant between pressure-broadened gaseous, weakly chemisorbed, and liquid states, provides quantification of sensitivity. A minimum detectable coverage of ~ 0.04 monolayer is determined at a weakly absorbed probe wavelength. © 1997 Elsevier Science B.V.

1. Introduction

The photon decay time of an optical cavity has been used to characterize intrinsic cavity losses for many years [1]. O'Keefe and Deacon [2] extended this strategy to the measurement of optical absorption spectra of gases. Since the publication of their work in 1988, the field of cavity ring-down spectroscopy (CRDS) has expanded rapidly. A wide variety of applications to both spectroscopy [3–9] and kinetics [10–13] has appeared. Innovations in the measurement technology have included extension to the ultraviolet [14] and infra-red regions [15], Fourier transform CRDS [16], and several strategies for employing cw sources [17–19]. Yet in general the technique has only been applied to the gas phase. Extension to condensed phases requires new cavity

designs that circumvent the introduction of additional intrinsic losses, while maintaining a well-defined relationship between absorption loss and photon decay time. We recently explored a novel implementation of the CRDS concept that utilizes a broadband, total-internal-reflection-ring cavity to extend CRDS to surfaces, thin films, and condensed matter in general [20]. This Letter describes the first experimental results in which CRDS is used to probe a surface process and the first demonstration of a CRDS cavity that incorporates intra-cavity total-internal reflection (TIR).

The use of intra-cavity TIR has many advantages for CRDS. TIR is a broadband process with an efficiency that is limited only by surface-roughness-induced scattering, if non-specular losses can be neglected [21]. Evanescent waves, which are required to satisfy the boundary conditions on Maxwell's equations, arise as a natural consequence

---

[1] National Research Council postdoctoral associate/NIST.

of TIR. The use of evanescent waves for probing optical absorption forms the basis for attenuated total reflectance (ATR) spectroscopy [22], which has permitted the solution of many diagnostic problems that are intractable by transmission methods. Enhancement of sensitivity by the use of a waveguide or other TIR element that permits multiple reflections is typically required in ATR spectroscopy due to the inherently large minimum detectable absorbance change per reflection. Yet for surface and thin-film diagnostics, ATR offers substantial advantages over transmission methods, since the electric field intensity at the TIR interface can be strongly enhanced and since interference fringes, which can obscure small absorbance changes in transmission experiments, are eliminated. Similar to transmission measurements, light source fluctuations and detector noise limit the ultimate performance of an ATR spectrometer. The CRDS technique provides a strategy for circumventing the effect of light source fluctuations, since the absorption rate for individual laser pulses is used instead of a ratio of optical powers. By constructing a CRD cavity that incorporates intra-cavity TIR, the advantages of an evanescent wave technique can be combined with the enhanced detection capability of CRDS to effectively extend ATR into the trace analysis regime.

In this work, the detection and characterization of a surface process by evanescent wave CRDS is accomplished with a cavity design that incorporates a 'superpolished', high-purity fused-silica Pellin-Broca prism which provides a single intra-cavity TIR per pass. Adsorption of I_2 at the TIR surface, which is external to the cavity, is detected and characterized. Based on the estimated cross-section for adsorbed I_2 at 625 nm and the calculated surface electric field enhancement, a minimum detectable coverage of 0.04 monolayer is determined.

2. Experimental

The optical configuration, which forms a stable resonator with intra-cavity TIR, is depicted in Fig. 1. The cavity consists of two concave, dielectric mirrors (Newport 10CV00-SR.30F, 1 m radius of curvature) with reflectivity of $\sim 99.99\%$ at 620 nm and a fused-silica (Corning 7940) Pellin-Broca prism (CVI
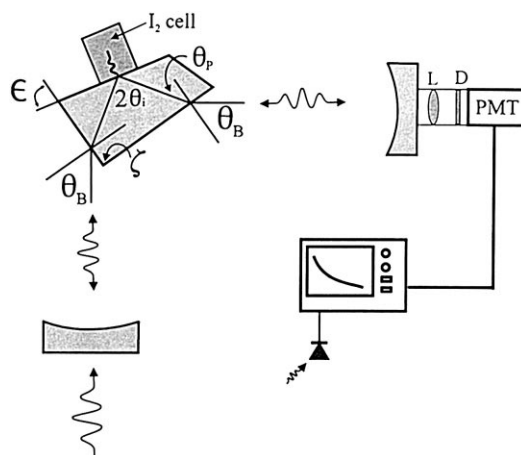

Fig. 1. A stable cavity is depicted that incorporates intra-cavity total-internal reflection (TIR) to permit surface processes to be probed by cavity ring-down through absorption of the associated evanescent wave. The cavity is formed from high-reflectivity, dielectric mirrors and a superpolished, fused-silica Pellin-Broca prism, which has high transmission for light polarized in the plane of the cavity. A 20 ns laser pulse is injected through a cavity mirror to excite cavity modes which decay at a rate that is determined by the ratio of the round-trip time to the round-trip losses as described by Eq. (1). To minimize transverse mode beating the output of the cavity is focussed by lens L onto diffuser plate D prior to striking the PMT detector. The scope is triggered by a photodiode.

Laser) which has a 632.8 nm design wavelength. The prism was positioned on a two-axis tilt table with a rotation axis normal to the plane of the cavity so that the rotation axis corresponded to the line formed by the intersection of the TIR plane surface and the plane bisecting the angle ζ [23] in Fig. 1. To minimize stress-induced birefringence, light clamping pressure was used in mounting the prism. The cavity mirrors were symmetrically separated from the prism by 46 cm, which provided a beam waist radius at the TIR surface of ~ 300 μm for the lowest-order cavity mode. The Rayleigh range for this configuration is ~ 44 cm, which provides nearly planar wavefronts at the Brewster angle surfaces, as well as at the TIR surface. The output of an excimer-pumped, dye laser using Sulforhodamine 640 was passed through a Glan-laser prism prior to entering the cavity to provide horizontally polarized light with an extinction ratio of $< 10^{-3}$. The beam path inside the cavity was enclosed and purged with dry nitrogen. A nondegenerate cavity length was used without

mode-matching of the input beam, resulting in the efficient excitation of transverse modes with mode indices $n,m \lesssim 6$, which is estimated from a comparison of the beam diameter at the input mirror to the mode half-widths for the Hermite–Gaussian modes [24]. The cavity output was detected by a photomultiplier tube (Hammamatsu R955HA, wired for < 1 ns rise time [13]) located behind the second mirror. All light exiting the cavity was efficiently collected, passed through a diffuser plate, and focused onto the PMT to minimize mode beating [25]. The output of the PMT was digitized by an 8-bit, 500 MS/s oscilloscope (LeCroy Model#9374) with a 25 MHz bandwidth-limiting filter and transferred to a microcomputer for processing. The bandwidth-limiting filter was applied to smooth longitudinal mode-beating thereby yielding essentially pure, single-exponential-decay waveforms for p-polarized input. The individual waveforms were fitted using a weighted, exponential fitting routine to extract the

decay times. Each point was obtained as an average of 25 decay times. Typically, a 0.2% standard deviation was obtained for data sets in which each point was a 25 shot average. A representative, unfiltered ring-down decay is shown in Fig. 2.

As a result of exposure to the ambient laboratory atmosphere and general handling, the base ring-down time for the cavity degraded slowly over time due to the accumulation of absorbing or scattering matter on the ultrasmooth surfaces. Although other strategies may be equally suitable, we used a three-step cleaning procedure involving: (1) the 'drop-and-drag' method with ultrahigh-purity methanol (< 0.1 ppm residue after evaporation) to remove particulates; (2) followed by swabbing with an ultrahigh-purity water/acetone saturated, binderless cotton swab; (3) followed by a final drop and drag with ultrahigh-purity methanol to remove the residual water. The original base loss of the system was restored by using this procedure.
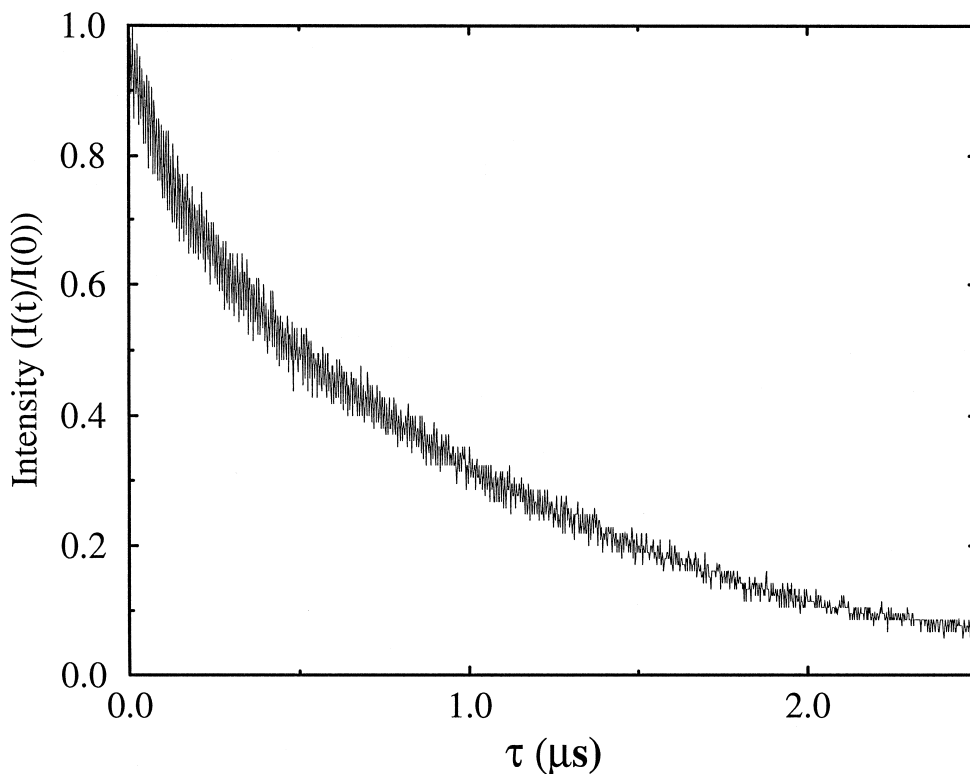

Fig. 2. A typical, unfiltered ring-down decay curve obtained with the cavity of Fig. 1 is shown. For p-polarized input, nearly pure, single exponential decay waveforms are obtained after filtering. The unfiltered data show longitudinal mode beating.

The angle of incidence at the TIR surface for the Pellin-Broca prism is 45°, which is close to the critical angle of 43.34° at the design wavelength. This close proximity to the critical angle maximizes the surface electric field intensity enhancement [22], but restricts this cavity design to diagnostics of surface and thin-film phenomena, since bulk media will frustrate the total reflection. However, since the critical angle is essentially independent of the film refractive index for films that are thin relative to the evanescent wave decay length of ~ 0.6 μm, a wide variety of thin-film systems can be studied. Adsorption of I_2 was examined by contacting a cell containing solid I_2 at the TIR facet as shown in Fig. 1. Sufficient solid I_2 was used in the cell to assure that equilibrium was rapidly established between the solid and vapor thereby providing a constant I_2 dosing pressure as established by the solid/vapor equilibrium. The vapor pressure of solid I_2 was 37 Pa (0.28 Torr) [26] at the ambient temperature of 22.4 ± 0.1°C during the experiment. The cell dimensions (1.0 cm $\times$ 2.3 cm $\times$ 5.0 cm) where large compared to the sampled area, which is determined by the ~ 300 μm beam waist at the TIR surface, so that the area being probed experienced uniform dosing conditions.

Intra-cavity TIR introduces new intrinsic losses that are not encountered in gas-phase CRDS cavities, such as bulk attenuation and polarization-dependent losses. In analogy to gas-phase CRDS, the photon decay time can be expressed in terms of the round-trip time, t_r, and the cavity losses according to

$$\tau(\omega)$$

$$= \frac{t_r}{2(1-R) + \mathscr{L}_{bulk} + \mathscr{L}_{surf} + \mathscr{L}_{pol} + 2\Gamma\sigma(\omega)N_s},$$
(1)

where R is mirror reflectivity, $\mathscr{L}_{bulk}$ is the prism bulk attenuation, $\mathscr{L}_{surf}$ is the prism surface scattering loss, $\mathscr{L}_{pol}$ is the total polarization-dependent loss, and $\sigma(\omega)$, Γ, and N_s are the absorption cross-section, surface field intensity enhancement, and number density for the adsorbed species, respectively. Diffraction losses have been neglected in Eq. (1), since the apertures associated with the mirrors and prism are very large relative to the transverse profiles of the fundamental and significantly excited higher-order modes [25]. Nonspecular losses have also been neglected, since the angle of incidence is sufficiently separated from the critical angle to reduce nonspecular transmission to a negligible level [20]. Bulk attenuation is estimated to be 640 ppm per round trip at 625 nm based on transmission data for Corning 7940 fused silica (~ 80 ppm/cm) [27]. The surface scattering loss per round trip that is introduced by the Pellin-Broca prism can be estimated from [28]

$$\mathscr{L}_{surf} = 2\sum_{i=1}^{3}\mathscr{L}_i = 2\sum_{i=1}^{3}\left(\frac{4\pi n_i \sigma_{RMS}\cos\theta_i}{\lambda_0}\right)^2, \quad (2)$$

where $\mathscr{L}_i$ is the surface scattering loss per surface, σ_{RMS} is the root-mean-square (rms) surface roughness, n_i is the incident-medium index of refraction, θ_i is the angle of incidence, and λ_0 is the vacuum wavelength. From Eq. (2) the round-trip surface scattering loss is found to be 5.4 ppm for the superpolished prism with $\sigma_{RMS} = 0.05$ nm. This is to be contrasted with the 418 ppm loss calculated for the prism prior to superpolishing which had a measured $\sigma_{RMS} = 0.44$ nm.

When bulk attenuation, surface scattering, and mirror losses are sufficiently small, the intrinsic cavity loss is largely determined by polarization-dependent losses. The Pellin-Broca prism provides high transmission for p-polarized light near the design wavelength, since light enters and exits the prism at or near Brewster's angle. The total polarization loss can be decomposed into in-plane and out-of-plane losses with respect to the plane of the cavity according to

$$\mathscr{L}_{pol} = \mathscr{L}_{pol}^{\parallel} + \mathscr{L}_{pol}^{\perp}, \quad (3)$$

where $\mathscr{L}_{pol}^{\parallel}$ arises from inaccuracies in the angles ζ and ϵ in Fig. 1 that introduce deviations from concurrent Brewster angle input and output, and $\mathscr{L}_{pol}^{\perp}$ arises from deviations in the plane of polarization from the ideal p-polarized state which are introduced by pyramidal error and polarization properties of the optical elements.

The in-plane loss per round trip that is introduced by inaccuracies in the angles ζ and ϵ can be estimated by assuming an incident plane wave, expanding the reflectivity for p-polarized light in a Taylor

series around the Brewster angle, and truncating after the first non-zero term to obtain

$$
\mathscr{L}_{\mathrm{pol}}^{\parallel} \approx 2 \sum_{i}^{\theta_{\mathrm{B}}, \theta_{\mathrm{P}}} \left| \frac{\partial R_{\parallel}(\theta_i)}{\partial \theta}(\theta - \theta_i) \right|^2
$$

$$
= 2 \left[\left(\frac{1 - n^4}{2n^3} \right)^2 (\Delta\theta_{\mathrm{B}})^2 + \left(\frac{1 - n^4}{2n} \right)^2 (\Delta\theta_{\mathrm{P}})^2 \right]
$$

$$
= \left(\frac{1 - n^4}{n} \right)^2 (\Delta\chi)^2, \qquad (4)
$$

where $R_{\parallel}(\theta_i)$ is the p-polarization amplitude reflectivity, $\Delta\theta_{\mathrm{B}}$ and $\Delta\theta_{\mathrm{P}}$ correspond to the deviations from Brewster's angle for the air/fused-silica and fused-silica/air interfaces, respectively, under optimal alignment conditions (limited by the fabrication error), and $\Delta\chi = 2\Delta\epsilon + \Delta\zeta$. Note that if the errors $\Delta\epsilon$ and $\Delta\zeta$ both lead to larger or smaller values for ζ and ϵ, the error will accumulate. For the Pellin-Broca, the angle ζ is a right angle, while ϵ is dependent on the prism refractive index, which is $n = 1.457018$ at the design wavelength of 632.8 nm, so that the target values for ζ and ϵ were 90.000° and 79.463°, respectively. These angles and the pyramidal error where corrected during the superpolishing process to within ± 5 arc minutes of the target values. According to Eq. (4), this leads to a maximum contribution to the round trip loss of 110 ppm, assuming maximum error accumulation.

The out-of-plane polarization loss arises from stress birefringence, pyramidal error, and depolarization by the concave, multilayer dielectric mirrors which result in the generation of an s-polarization component that is efficiently rejected by the Brewster angle facets of the Pellin-Broca. Stress birefringence exists as an inherent material property, but can also be introduced by mounting. The polishing process also introduces birefringence through the generation of micro-crystalline cracks that propagate into the clear aperture from the prism edges, which is relieved by an acid etch [29] of the unpolished surfaces. Pyramidal error arises when the surface normals of the input, TIR, and output facets of the Pellin-Broca deviate from the same plane. Mirror curvature and coating properties can also lead to polarization scrambling. If the angle of the electric field relative to the plane of the cavity is δ, we find that the out-of-plane polarization loss is given by

$$
\mathscr{L}_{\mathrm{pol}}^{\perp} = 2 \sum_{i}^{\theta_{\mathrm{B}}, \theta_{\mathrm{P}}} \left| R_{\perp}(\theta_i) \right|^2 \sin^2 \delta_i
$$

$$
= 2 \left| \frac{1 - n_i^2}{1 + n_i^2} \right|^2 \left(\sin^2 \delta_{\theta_{\mathrm{B}}} + \sin^2 \delta_{\theta_{\mathrm{P}}} \right), \qquad (5)
$$

where $R_{\perp}(\theta_i)$ is the s-state amplitude reflectivity, and θ_{B} and θ_{P} are the incident angles at the rarer $\rightarrow$ denser and denser $\rightarrow$ rarer interfaces, respectively, where the reflectivities and polarization angles are evaluated. A detailed model could be developed for δ as a function of position in the cavity using a Jones matrix formulation [30], but ultimately accurate characterization of the particular optical components becomes necessary to assess small losses. The contribution of stress birefringence to the total loss will be substantially reduced through the use of a smaller prism which is fabricated from a selected grade of material.

3. Results and discussion

To demonstrate detection of adsorbed I_2 by evanescent wave CRDS, exposure of the Pellin-Broca TIR surface to I_2 vapor was cycled as shown in Fig. 3, where the total cavity loss is plotted for four adsorption and desorption cycles. The step-function-like changes result from a 3 min equilibration time following exposure or removal of the I_2 cell, during which acquisition was halted. For each adsorption or desorption phase, data were collected for 6 min at a 10 Hz repetition rate with 25 shots averaged per point. Results for two wavelengths, 625 and 660 nm, are shown, corresponding to the upper and lower waveforms, respectively. The sensitivity for probing the adsorption is greater at 625 nm compared to 660 nm as revealed by the difference in the slopes of the adsorption curves. As discussed below, this difference arises from the difference in absorption cross-section at these wavelengths for the $^1\Sigma_{\mathrm{g}}^{+} \rightarrow {}^3\Pi_{\mathrm{u}}$ transition of I_2, which in the gas phase has an absorption maximum at 520 nm with $\alpha_{520\ \mathrm{nm}} = 2.56 \times 10^{-18}$ cm^2/molecule [31], but other origins for this signal
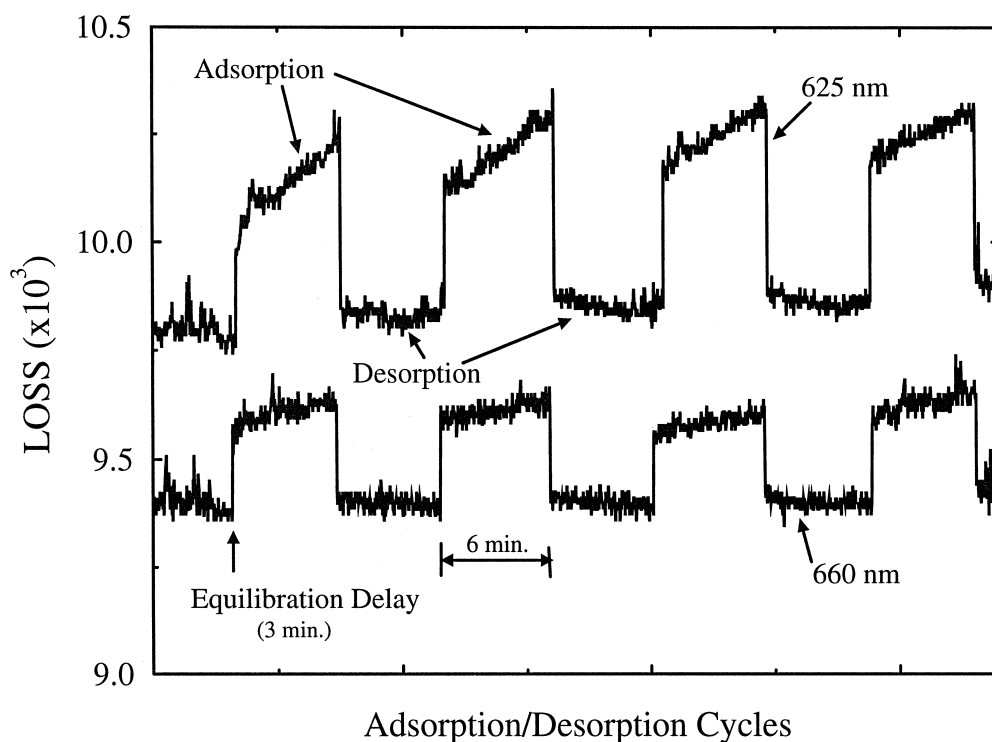
Fig. 3. The reversible adsorption of I_2 on the superpolished fused silica TIR surface is demonstrated at two wavelengths by measuring the increased cavity loss resulting from sub-monolayer adsorption. Four typical adsorption/desorption cycles are shown to illustrate reversibility and repeatability for each wavelength. The step-like changes result from stopping the acquisition to allow equilibration. The larger slope detected at 625 nm compared with 660 nm arises from the larger absorption cross-section at 625 nm. The small difference in base loss at the two wavelengths arises from the weak dependence of photon decay time on wavelength over this range.

change are worth considering. Polarization scrambling cannot account for the increase in cavity loss with adsorption, since for an isotropic (or anisotropic, uniaxial) adlayer, the s- and p-polarization states remain orthogonal [32]. An increase in surface scattering could contribute to the change in cavity loss with adsorption through an increase in the surface rms roughness, δ_{RMS}. However, if the increase in δ_{RMS} is assumed to be bounded above by the Van der Waals radius of I_2, then from Eq. (2) for the TIR surface, the increase in surface scattering loss due to adsorption can be estimated to be at most 5% of the total loss change. Furthermore, a much weaker dependence on wavelength would be expected then is found in Fig. 3. Indeed, evanescent wave spectroscopy is frequently used to probe highly scattering materials due to an increased resistance to scattering in comparison to transmission measurements. In ad-

dition, the results of Fig. 3 do not correspond to gas-phase absorption, since for the I_2 vapor pressure of 37 Pa (0.28 Torr) and with an evanescent wave decay length of ~ 600 nm, an absorbance change of < 0.1 ppm is expected, which is well below the minimum detectable change for this experiment.

To quantify the sensitivity of evanescent wave CRDS in the form of a minimum detectable coverage, values for the surface electric field intensity enhancement and the absorption cross-section of adsorbed I_2 are needed. Since the absorption cross-section of the adsorbed form could differ significantly from I_2 in other states, a reliable estimation of this value is critical. Fortunately, the adsorption of I_2 on silica gel has been studied [33], which provides information on spectral changes and coverage. From Fig. 3, it is apparent that the interaction between I_2 and fused silica approaches equilibrium on a time

scale of minutes. Fig. 4 shows an adsorption curve over a much longer time period than Fig. 3, which reveals the asymptotic approach to an equilibrium coverage, Θ_e. Given a value for the cross-section and the field intensity enhancement, an estimate of the I_2 equilibrium coverage can be obtained, which can be compared with studies on silica gel, since the value of Θ_e for the TIR facet of the fused-silica prism can be expected to be similar.

The inset in Fig. 4 shows the calculated surface electric field and total field intensity enhancements at the fused-silica/air TIR interface where the xz-plane is the plane of incidence and the z-axis is normal to the interface. At 45° the total field intensity enhancement is ~ 7.4, which is dominated by enhancement of the z-component of the field. Therefore, adsorbates with transition dipoles that are oriented perpendicular to the surface will experience the maximum field enhancement. These calculations,

which are based on the Fresnel equations, are exact within the local dielectric approximation, although the effect of the adsorbate has been neglected. Estimation of the absorption cross-section of the adsorbate might ordinarily be less certain. However, in the visible region the absorption spectra of I_2 for the pressure-broadened gas-phase [31], the liquid phase near the critical point [34], or weakly chemisorbed on silica gel [33], differ only slightly. The invariance of the absorption coefficient and line shape with increasing I_2 density can be understood by recognizing that the interaction between I_2 molecules is dominated by a $\pi \rightarrow \sigma^*$ intermolecular electron transfer, which significantly alters the UV absorption spectrum but has little effect on the intramolecular $^1\Sigma_g^+ \rightarrow {}^3\Pi_u$ transition. Furthermore, the influence of the intermolecular transition on the visible transition is especially weak on the long-wavelength side. Therefore, the gas-phase value for the absorption
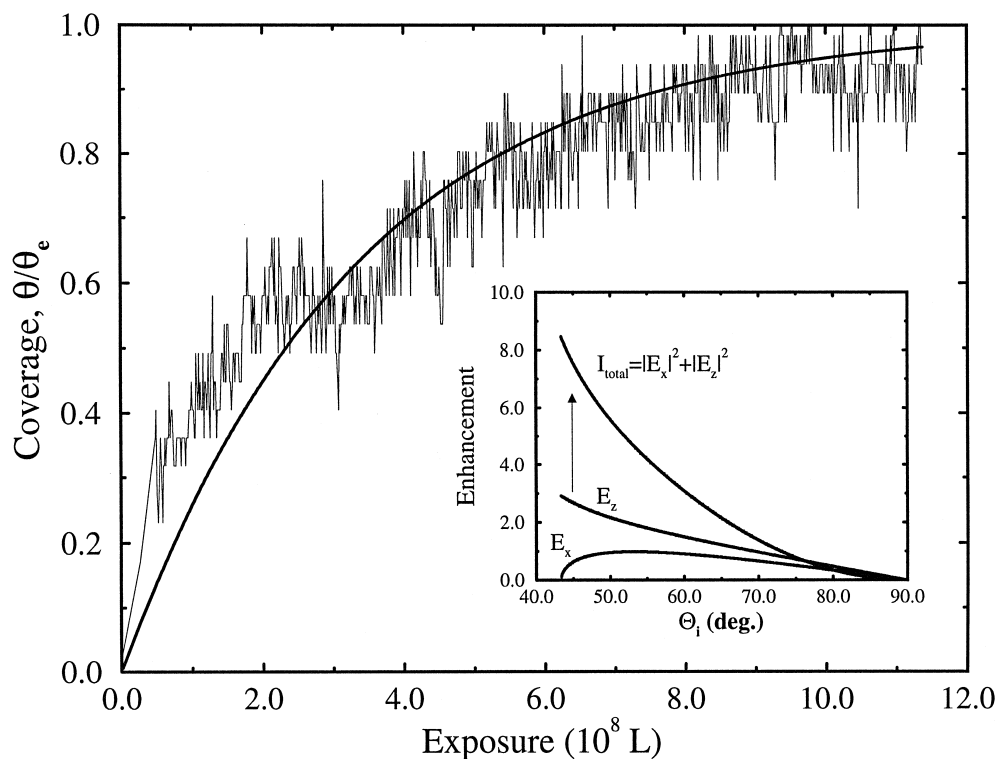

Fig. 4. Approximate Langmuir kinetics are observed for adsorption of I_2 on the ultra-smooth, fused-silica, TIR surface of the Pellin-Broca prism when probed at 625 nm. A long exposure $(1 L = 1 \times 10^{-6}$ Torr s $= 1.33 \times 10^{-4}$ Pa s$)$ is required to reach equilibrium coverage at the ambient temperature of 22.4°C. The inset shows the surface electric field intensity enhancement for the fused-silica/air interface as a function of angle of incidence. At 45° the enhancement is ~ 7.4. The (0,0) data point is included and a 3 min equilibration delay was used.

cross-section at the probe wavelength, which is estimated to be $\sigma_{625} = 2.5 \times 10^{-19}$ cm^2/molecule, can be used to extract Θ_e and the minimum detectable coverage of adsorbed I$_2$. It is important to note that the gas-phase value represents a lower limit that will underestimate the minimum detectable surface coverage, since any small degree of line broadening will at most enhance the cross-section at the edge of the absorption band. Therefore, assuming $N_o = 5 \times 10^{14}$ sites/cm^2 as the density of adsorption sites [33], Eq. (1) gives $N_s = 9.2 \times 10^{13}$ or $\Theta_e = 0.18$, which is larger than previous estimates [33,35] but consistent with the conclusion of a sub-monolayer equilibrium coverage. Similarly, the minimum detectable coverage is estimated to be 0.04 monolayer. These calculations utilize the maximum field enhancement factor, which assumes that I$_2$ is oriented normally to the surface, since the transition dipole is parallel to the molecular axis due to strong spin–orbit coupling [36].

The time dependence of adsorption shown in Fig. 4 also provides a potentially informative observable. The time dependence apparently does not arise from diffusion, since the effect is independent of the mass of solid I$_2$ in the cell beyond a threshold amount and the calculated estimate of mixing time is short relative to the equilibration time. The data of Fig. 4 appear to approximately correspond to Langmuir adsorption kinetics. Langmuir adsorption assumes that the sticking coefficient, s, is proportional to the fraction of open sites Θ, or $s = s(0)(1 - \Theta)$, where $s(0)$ is the zero coverage sticking coefficient, which yields a simple integrated rate law given by

$$\Theta(t) = \Theta_e(1 - e^{-kPt}) \qquad (6)$$

with

$$k = \frac{s_o a_s}{(2\pi m_{I_2} kT)^{1/2}} e^{E_a/k_b T}, \qquad (7)$$

where P is the I$_2$ pressure, a_s is the area per site, and m$_{I_2}$, k, and T are the I$_2$ molecular mass, Boltzmann constant, and absolute temperature, respectively, and the form

$$s(0) = s_o e^{E_a/k_b T}$$

has been assumed for the zero-coverage sticking coefficient. An approximate fit to the data of Fig. 4

yields $s(0) \approx 10^{-8}$. If $s_o = 1$, this implies $E_a \approx 0.5$ eV. However, since the desorption rate is apparently rapid compared to the adsorption rate based on the results of Fig. 3, a small pre-exponential factor as opposed to a large activation barrier more likely accounts for the small sticking coefficient. A small pre-exponential factor may arise from entropic effects associated with the presence of a water layer. A more detailed analysis would be required to resolve these issues.

4. Conclusions

CRDS with intra-cavity TIR has been demonstrated to be a very sensitive technique for probing surface processes. Since the length scale for the electric field decay (~ 100 nm) is long relative to the length scale for establishing the chemical response of a surface (~ 10 nm), evanescent wave CRDS can be used to study a wide variety of surface interactions. In comparison to electron spectroscopies, sub-monolayer sensitivity is readily achieved without the requirement of an ultra-high vacuum environment. In comparison with non-linear optical techniques, the greater simplicity of the method should provide significant advantages. Indeed through the development of lower intrinsic loss cavity designs, evanescent wave CRDS will likely provide a significant improvement over other linear optical techniques such as waveguide ATR as well. For example, a factor of 10^2 improvement in detection sensitivity over the results presented here can be expected with a square, monolithic, TIR-ring cavity, which eliminates polarization losses and minimizes bulk losses [20]. Furthermore, the results discussed here were obtained for a moderate absorber at a weakly resonant probe wavelength. Extension to the fingerprint IR region should also be especially powerful.

Disclaimer. Identification of specific commercial products in this paper is provided in order to specify procedures completely. In no case does such identification imply recommendation or endorsement by the National Institute of Standards and Technology, nor does it imply that such products have necessarily been identified as the best available for the purpose.

Acknowledgements

References

[1] O.E. Delange, Bell Syst. Tech. J. 44 (1965) 283.

[2] A. O'Keefe, D.A.G. Deacon, Rev. Sci. Instrum. 59 (1988) 2544.

[3] D. Romanini, K.K. Lehmann, J. Chem. Phys. 99 (1993) 6287.

[4] E.H. Wahl, T.G. Owano, C.H. Kruger, P. Zalicki, Y. Ma, R.N. Zare, Diamond Relat. Mater. 5 (1996) 373.

[5] D. Romanini, K.K. Lehmann, J. Chem. Phys. 105 (1996) 68.

[6] J. Pearson, A.J. Orr-Ewing, M.N.R. Ashfold, R.N. Dixon, J. Chem. Soc. Faraday Trans. 92 (1996) 1283.

[7] P. Zalicki, Y. Ma, R.N. Zare, E.H. Wahl, J.R. Dadamio, T.G. Owano, C.H. Kruger, Chem. Phys. Lett. 234 (1995) 269.

[8] J.J. Scherer, J.B. Paul, C.P. Collier, R.J. Saykally, J. Chem. Phys. 102 (1995) 5190.

[9] D.L. Huestis, R.A. Copeland, K. Knutsen, T.G. Slanger, R.T. Jongma, M.G.H. Boogaarts, G. Meijer, Can. J. Phys. 72 (1994) 1109.

[10] L. Zhu, D. Kellis, C.F. Ding, Chem. Phys. Lett. 257 (1996) 487.

[11] T. Yu, M.C. Lin, J. Phys. Chem. 99 (1995) 8599.

[12] E.W. Diau, T. Yu, M.A.G. Wagner, M.C. Lin, J. Phys. Chem. 98 (1994) 4043.

[13] D.B. Atkinson, J.W. Hudgens, J. Phys. Chem. A 101 (1997) 3901.

[14] G. Meijer, M.G.H. Boogaarts, R.T. Jongma, D.H. Parker, Chem. Phys. Lett. 217 (1994) 112.

[15] J.J. Scherer, D. Voelkel, D.J. Rakestraw, J.B. Paul, C.P. Collier, R.J. Saykally, A. O'Keefe, Chem. Phys. Lett. 245 (1995) 273.

[16] R. Engeln, G. Meijer, Rev. Sci. Instrum. 67 (1996) 2708.

[17] G. Meijer, R. Engeln, Chem. Phys. Lett. 262 (1996) 105.

[18] D. Romanini, A.A. Kacchanov, F. Stoeckel, Chem. Phys. Lett. 264 (1997) 316.

[19] B.A. Paldus, J.S. Harris, J. Martin, J. Xie, R.N. Zare, J. Appl. Phys. (in press).

[20] A.C.R. Pipino, J.W. Hudgens, R.E. Huie, Rev. Sci. Instrum. 68 (1997) 2978.

[21] J.J. Regan, D.R. Andersen, Comput. Phys. 49 (1991) (Jan./Feb.).

[22] N.J. Harrick, Internal Reflection Spectroscopy, Interscience, New York, 1967.

[23] J. Reader, Appl. Opt. 12 (1973) 1405.

[24] A.E. Seigman, Lasers, University Science Books, Mills Valley, CA, 1986.

[25] J.T. Hodges, J.P. Looney, R.D. Van Zee, J. Chem. Phys. 105 (1996) 10278.

[26] An.N. Nesmeyanov, Vapour Pressure of the Elements, Academic Press, New York, 1963.

[27] M.W. Jones, K.C. Kao, J. Phys. E 2 (1969) 331.

[28] O. Kienzle, J. Staub, T. Tschudi, Meas. Sci. Tech. 5 (1994) 747.

[29] C. Terpstra, private communication, Research Electro-Optics, Boulder, CO.

[30] R.A. Chipman, Opt. Eng. 28 (1989) 90.

[31] J.G. Calvert, J.N. Pitts, Jr., Photochemistry, Wiley, New York, 1967.

[32] R.M.A. Azzam, N.M. Basharsa, Ellipsometry and Polarized Light, North-Holland Publishing Co., New York, 1977.

[33] G. Kortum, H. Koffer, Ber. Bunsenges. Phys. Chem. 67 (1963) 67.

[34] I. Yamamoto, A. Tanaka, H. Endo, J. Non-Cryst. Solids 156-158 (1993) 728.

[35] T. Nagasao, H. Yamada, J. Raman Spectrosc. 3 (1975) 153.

[36] J.T. Hougen, private communication.